

Development of the oncolytic virus, CF33, and its derivatives for peritoneal-directed treatment of gastric cancer peritoneal metastases

Annie Yang,¹ Zhifang Zhang,¹ Shyambabu Chaurasiya,¹ Anthony K Park ,² Audrey Jung,¹ Jianming Lu,¹ Sang-In Kim,¹ Saul Priceman ,² Yuman Fong,¹ Yanghee Woo ¹

To cite: Yang A, Zhang Z, Chaurasiya S, *et al.* Development of the oncolytic virus, CF33, and its derivatives for peritoneal-directed treatment of gastric cancer peritoneal metastases. *Journal for ImmunoTherapy of Cancer* 2023;11:e006280. doi:10.1136/jitc-2022-006280

► Additional supplemental material is published online only. To view, please visit the journal online (<http://dx.doi.org/10.1136/jitc-2022-006280>).

AY and ZZ contributed equally.

Accepted 09 March 2023



© Author(s) (or their employer(s)) 2023. Re-use permitted under CC BY-NC. No commercial re-use. See rights and permissions. Published by BMJ.

¹Department of Surgery, City of Hope National Medical Center, Duarte, California, USA

²Cancer Immunotherapeutics Program, Beckman Research Institute, City of Hope National Medical Center, Duarte, California, USA

Correspondence to

Dr Yanghee Woo;
yhwoo@coh.org

Dr Zhifang Zhang;
zhzhang@coh.org

ABSTRACT

Background Gastric cancer (GC) that metastasizes to the peritoneum is fatal. CF33 and its genetically modified derivatives show cancer selectivity and oncolytic potency against various solid tumors. CF33-hNIS and CF33-hNIS-antiPDL1 have entered phase I trials for intratumoral and intravenous treatments of unresectable solid tumors (NCT05346484) and triple-negative breast cancer (NCT05081492). Here, we investigated the antitumor activity of CF33-oncolytic viruses (OVs) against GC and CF33-hNIS-antiPDL1 in the intraperitoneal (IP) treatment of GC peritoneal metastases (GCPM).

Methods We infected six human GC cell lines AGS, MKN-45, MKN-74, KATO III, SNU-1, and SNU-16 with CF33, CF33-GFP, or CF33-hNIS-antiPDL1 at various multiplicities of infection (0.01, 0.1, 1.0, and 10.0), and performed viral proliferation and cytotoxicity assays. We used immunofluorescence imaging and flow cytometric analysis to verify virus-encoded gene expression. We evaluated the antitumor activity of CF33-hNIS-antiPDL1 following IP treatment (3×10^5 pfu \times 3 doses) in an SNU-16 human tumor xenograft model using non-invasive bioluminescence imaging.

Results CF33-OVs showed dose-dependent infection, replication, and killing of both diffuse and intestinal subtypes of human GC cell lines. Immunofluorescence imaging showed virus-encoded GFP, hNIS, and anti-PD-L1 antibody scFv expression in CF33-OV-infected GC cells. We confirmed GC cell surface PD-L1 blockade by virus-encoded anti-PD-L1 scFv using flow cytometry. In the xenograft model, CF33-hNIS-antiPDL1 (IP; 3×10^5 pfu \times 3 doses) treatment significantly reduced peritoneal tumors ($p < 0.0001$), decreased amount of ascites (62.5% PBS vs 25% CF33-hNIS-antiPDL1) and prolonged animal survival. At day 91, seven out of eight mice were alive in the virus-treated group versus one out of eight in the control group ($p < 0.01$).

Conclusions Our results show that CF33-OVs can deliver functional proteins and demonstrate effective antitumor activity in GCPM models when delivered intraperitoneally. These preclinical results will inform the design of future peritoneal-directed therapy in GCPM patients.

BACKGROUND

Gastric cancer (GC) is a major global health burden affecting over one million people

WHAT IS ALREADY KNOWN ON THIS TOPIC

⇒ Despite the availability of standard-of-care treatments for gastric cancer peritoneal metastases (GCPM), including chemotherapy alone or combined with immunotherapy, these strategies have demonstrated modest survival benefits, and no durable responses are seen in the peritoneum.

WHAT THIS STUDY ADDS

⇒ We leveraged the potential of the oncolytic virus CF33 platform, engineered to express anti-PD-L1 scFv previously used in treating unresectable solid tumors. We tested the antitumor effects of CF33-hNIS-antiPDL1 in GCPM in vitro and in vivo. We demonstrate robust antitumor effects in vitro and safety and efficacy after intraperitoneal CF33-hNIS-antiPDL1 treatment, followed by tumor regression and prolonged animal survival in a xenograft GCPM mouse model.

HOW THIS STUDY MIGHT AFFECT RESEARCH, PRACTICE OR POLICY

⇒ For the first time, our preclinical results demonstrate a significant therapeutic potential for CF33-oncolytic viruses in treating GCPM, for which there are currently no durable therapies.

yearly.¹ While significant variability in the incidence, stage at the time of initial presentation, and national mortality rates exist, GC remains the fourth-leading cause of cancer-related deaths after lung, colorectal, and liver cancers, with 769,000 GC patient deaths estimated in 2020 worldwide.^{1,2} As in Europe, South America, and China, majority of GC patients in the USA present in advanced stages,³ where systemic therapy has become an integral part of the standard of care (SOC) best practices both, for patients with locally advanced disease undergoing curative-intent surgery, or those with unresectable or metastatic disease receiving a combination

of chemotherapeutic agents with or without biomarker targeted agents.^{4–7} The adoption of optimized surgical techniques and more effective systemic regimens have improved the 5-year overall survival of GC patients from 25% in 2012 to over 40% in 2021.⁸ However, treatment resistance and systemic treatment-related toxicities limit therapeutic durability resulting in distant recurrences and progression of the disease. Novel therapeutic strategies are sought to improve survival and decrease treatment-related side effects.

Peritoneal metastasis (PM) is the most common end-stage manifestation of GC for which systemic strategies have limited efficacy.^{7,9} GCPM affects over 40% of patients at the initial time of diagnosis or recurrence and 60% of all GC patients at the time of death.^{7,9} GC patients who develop PM often progress within 3 months of first-line systemic therapies. The addition of peritoneal-directed regional strategies has been sought to address therapeutic challenges posed by the diffuse nature of peritoneal tumors that progress unchecked in an immune-privileged peritoneal tumor microenvironment (TME) protected by the blood–peritoneal barrier.⁷ The extent of peritoneal tumor burden can range from occult cytology-positive disease to organ-encasing carcinomatosis, while therapeutic failures ultimately result in a myriad of complications, such as malignant bowel obstruction, malignant ascites, cachexia, and death within 2–11 months.^{7,10,11} With a dismal 5-year overall survival of less than 2%, GCPM remains a significant therapeutic challenge and an unmet cancer care need.^{12–17}

While primary GC are molecularly heterogeneous, peritoneal GC tumors are often histologically diffuse, genomically stable, immunogenically inactive, and remain refractory to the improving arsenal of systemic regimens, including biomarker-selected agents currently approved for GC.^{7,18–21} Early-phase monotherapy trials in patients with unresectable or metastatic GC, treated with trastuzumab (antitumor-specific human epidermal growth factor 2, anti-HER-2),²² ramucirumab (antivascular endothelial growth factor),^{23–25} and immune checkpoint inhibitors (ICIs) that block the programmed cell death 1/programmed cell death ligand 1 (PD-1/PD-L1) pathways, including pembrolizumab (anti-PD-1),^{26–30} and nivolumab (anti-PD-1) initially failed to demonstrate efficacy.^{31–33} While these immunotherapeutic agents, combined with chemotherapy, have achieved modest survival benefits compared with chemotherapy alone, few robust responses are seen in the peritoneum and with limited therapeutic durability.^{32,34}

Oncolytic virotherapy is a versatile treatment modality with both diagnostic and therapeutic capacity in solid tumors with the potential to improve GCPM patient outcomes. Oncolytic viruses (OVs) are designed to selectively infect malignant tumors, hijack the DNA of cancer cells by intracellular replication, and eventual oncolysis for tumor destruction. This mechanism of action allows for intratumoral (IT) or peritumoral transgene expression of desired proteins and subsequent oncolysis of

infected cancer cells without causing harm to normal tissues.³⁵ A new class of engineered vaccinia viruses has become an attractive anticancer agent with an excellent safety profile in multiple phase I studies.^{36–38} Previously, we demonstrated the safety, efficacy, and antitumor immune activity of CF33 and its derivatives (CF33-OVs) engineered to express GFP (CF33-GFP), human sodium/iodide symporter (CF33-hNIS), and both hNIS and anti-PD-L1 scFv (CF33-hNIS-antiPDL1) in breast cancer, colon cancer, lung cancer, and pancreatic adenocarcinomas.^{39–46} Having completed rigorous preclinical studies for IT and intravenous delivery of CF33-OVs, CF33-hNIS (VAXINIA, Imugene, Sydney, Australia), and CF33-hNIS-antiPDL1 (CheckVacc, Imugene, Sydney, Australia) entered phase I trials for IT and intravenous treatment of unresectable solid tumors, and IT treatment of triple-negative breast cancer (TNBC), respectively. To translate CF33-OVs into an effective therapeutic strategy for GCPM patients, we investigated the antitumor activity of CF33-OVs against GC. This study demonstrates robust and reproducible antitumor activities of CF33-OVs in GC in vitro and the safety and efficacy of intraperitoneal (IP) CF33-hNIS-antiPDL1 treatment of GCPM in xenograft models in vivo.

METHODS

Generation of CF33 and its variants

CF33, CF33-GFP, CF33-hNIS-ΔF14.5L (CF33-hNIS-Δ), and CF33-hNIS-antiPDL1 were evaluated in this study. The generation of CF33 and its sequenced genome has been previously described.^{38,39,42} In brief, CF33 is the chimeric virus without genetic modification. CF33-GFP has been genetically engineered by inserting a *GFP* cassette in the *J2R* locus. CF33-hNIS-Δ gene has the *hNIS* cassette inserted in the *J2R* locus with deletion of the *F14.5L* gene, while CF33-hNIS-antiPDL1 has the addition of *single chain anti-PD-L1 cDNA* inserted into the *F14.5L* gene under vaccinia H5 early promoter control.

Cell culture and cell lines

Human GC cell lines, AGS (ATCC, catalog# CRL-1739), KATO III (ATCC, catalog# HTB-103), MKN-74 (ACCEGEN, catalog# ABC-TC0689), MKN-45 (ACCEGEN, catalog# ABC-TC0687), SNU-1 (ATCC, catalog# CRL-5971), SNU-16 (ATCC, catalog#CRL-5974) and African green monkey kidney fibroblast CV-1 (ATCC, catalog# CCL-70) were purchased from the American Type Culture Collection (ATCC, Manassas, Virginia, USA) or ACCEGEN (Fairfield, New Jersey, USA). KATO III, MKN-74, MKN-45, SNU-1, and SNU-16 were cultured in RPMI medium 1640. AGS and CV-1 were cultured in DMEM. Unless stated otherwise, culture media was supplemented with 10% fetal bovine serum (FBS) and 1% antibiotic-antimycotic solution. All the media and supplements were purchased from Corning (Corning, New York, USA). Cells were maintained in a humidified incubator at 37°C and 5% CO₂.

Virus infection and proliferation assay

AGS, KATO III, MKN-74, MKN-45, SNU-1, and SNU-16 cells were plated in 6-well plates at 5×10^5 cells/well and incubated overnight. The next day, cells were counted and infected with viruses (CF33, CF33-GFP, CF33-hNIS- Δ , or CF33-hNIS-antiPDL1). Briefly, media from the wells was removed, and virus diluted in a medium containing 2.5% FBS was added to each well in a total volume of 0.5 mL such that the ratio of cells to the virus was 100:1, that is, a multiplicity of infection (MOI) of 0.01 plaque-forming units (pfu)/cell. Cells were incubated at 37°C for 1 hour, followed by aspiration of inoculum and addition of 2 mL media containing 10% FBS to each well. Plates were then returned to the incubator. Cell lysates were collected by scraping at 24 hours, 48 hours, and 72 hours, and virus titers in the lysates were determined by the standard plaque assay technique described previously.³⁹ All experiments were repeated at least three times.

Cytotoxicity assay

Cells were seeded at 3000 cells/well in 96-well plates with 100 μ L/well of medium supplemented with 10% FBS and incubated overnight. Virus was thawed on ice and sonicated for 1 min, and appropriate MOIs (0, 0.01, 0.1, 1.0, and 10.0) were calculated and prepared for infection in a medium with 2.5% FBS for 20 μ L/well. Cell viability relative to mock-infected cells was measured in triplicate every 24 hours for 8 days using an MTS cell proliferation assay with CellTiter 96 Aqueous One solution (Promega, Madison, Wisconsin, USA) on a spectrophotometer (Tecan Spark 10M, Mannedorf, Switzerland) at 490 nm. All experiments were repeated at least three times.

GFP fluorescent imaging in vitro

AGS, KATO III, MKN-74, and MKN-45 cells were plated in 24-well plates at 2×10^5 cells/well and incubated overnight. The next day, cells were counted and infected with CF33-GFP at an MOI of 1 and 0.01. Cells were imaged for virus-encoded GFP using a fluorescence microscope every 24 hours postinfection for 8 days.

Flow cytometry

Human GC cell lines AGS, MKN-45, MKN-74, KATO III, SNU-1, and SNU-16 (5×10^5 cells) were either directly harvested for staining or co-cultured with CF33-hNIS- Δ (MOI=3), CF33-hNIS-antiPDL1 (MOI=3), or phosphate buffered saline (PBS) (control) for 15 hours. Then, cells were harvested for surface and intracellular CD274/PD-L1 expression. For cell surface staining, cells were washed with PBS, blocked with 10% human serum in PBS, stained with PE-isotype control (Biolegend, Cat#402204, clone#27-35) or PE-anti-PD-L1 antibody (Biolegend, Cat#329706, clone#29E.2A3), washed thrice with 2% FBS PBS, and analyzed with a BD LSRFortessa Flow Cytometer (BD Biosciences, San Jose, California, USA). In the virus-treated group, cells were fixed with 4% paraformaldehyde before performing flow cytometry. For intracellular staining, cells were first washed with PBS and blocked with 10% human

serum. Then the cells were fixed/permeabilized with a fixation/permeabilization solution (Catalog#554714, BD Biosciences) for 20 min, washed twice with BD Perm/Wash buffer, stained with antibodies for 30 min, and washed twice with BD Perm/Wash buffer. Stained cells were assessed with a BD LSRFortessa Flow Cytometer and analyzed using Flowjo software. Results are shown as histograms and mean fluorescence intensity (MFI).⁴⁷ All experiments were repeated at least three times.

Immunofluorescence microscopy

AGS and MKN-45 cells (5×10^5 cells) were cultured with CF33-hNIS- Δ (MOI=3), CF33-hNIS-antiPDL1 (MOI=3), or PBS (control) for 18 hours. Cells were harvested, blocked with 10% human serum, fixed/permeabilized with BD fixation/permeabilization solution, and stained with primary antibodies (mouse anti-human NIS antibody, EMD Millipore catalog#MAB3564, clone#FP5A; mouse isotype control antibody, Biolegend catalog#402202, clone#27-35; rat anti-FLAG-tag antibody, Biolegend catalog#637304, clone# L5; rat isotype control antibody, Biolegend catalog#402302, clone#G013C12) for 30 min. After washing with washing buffer, cells were stained with secondary Alexa 488 or 555 conjugated antibodies (goat anti-mouse IgG(H+L)-Alexa 488, Invitrogen catalog# A11029, and goat anti-rat IgG(H+L)-Alexa 555, Invitrogen catalog# A21434) for 30 min. After washing, cells were mounted with Hard Set Mounting Medium with DAPI (Catalog# H-1500, Vector Laboratories, Burlingame, California, USA). Images were acquired on a Zeiss LSM 880 confocal microscope using Zen Black and a 20 \times /0.8 NA PlanApochromatic objective at a spatial resolution of 0.42 μ m/pixel and frame size 1024 \times 1024. The excitation and emission were red 594 nm excitation and 600–650 nm emission, green 488 nm excitation, and 500–550 nm emission, and blue 405 nm excitation and 410–490 nm emission via PMT detectors. Images were adjusted for brightness in a linear manner using Zen Blue V.2.3 software, and all images were adjusted identically.⁴⁰

Establishment of SNU-16-ffluc cell lines

To quantitate tumor volume and dissemination in vivo using non-invasive optical imaging (Xenogen), SNU-16 cells were modified to stably encode firefly luciferase using lentiviral transduction. Briefly, SNU-16 cells were incubated with polybrene (4 mg/mL, Sigma) in RPMI-1640 (Lonza catalog# BE12-702F) containing 10% FBS (Hyclone defined FBS, Cytiva catalog# SH30070.03), and 1X antibiotic-antimycotic (Gibco catalog#15240062) and infected with lentivirus carrying ffluc cDNA under the control of the EF1 α promoter. Expression of ffluc in SNU16 cells was confirmed, and single-cell subcloning was performed by the limiting dilution method.⁴⁸

Animal model of peritoneal dissemination xenograft of GCPM of SNU-16-ffluc cells

Six-week-old Hsd:ATHymic Nude-Foxn1nu female and male mice (Envigo, Indianapolis, Indiana, USA) were purchased and acclimatized for 2 weeks. To allow for

imaging of peritoneal tumor burden and evaluate the effect of IP CF33-hNIS-antiPDL1 in GCPM, a peritoneal xenograft mouse model was generated by peritoneal injection of SNU-16-ffluc cells. Injection of 10^7 SNU-16-ffluc cells in a total volume of 100 μ L PBS into the peritoneal cavity was performed for each mouse.

Bioluminescence imaging as a measure of tumor burden

Because caliper measurement is not feasible for measuring peritoneal tumor burden, we used bioluminescent imaging as a surrogate for tumor burden, as previously described.^{49 50} All animals were imaged with bioluminescence for luciferase activity in the peritoneum to identify peritoneal tumor implants and growth after IP SNU-16-ffluc, and the tumor burden was quantified once a week after treatment. D-luciferin solution was prepared by dissolving 1 g of IVISbrite D-Luciferin Potassium Salt Bioluminescent Substrate (PerkinElmer, catalog#122799-5, Waltham, Massachusetts, USA) in 35 mL of PBS at 28.5 mg/mL concentration. IP delivery (200 μ L/mouse) was performed in all groups, and the mice were imaged using Lago X optical imaging system (Spectral Instruments Imaging, Tucson, Arizona, USA). Bioluminescence imaging was analyzed using Aura V.64 software and presented as photons/second for regions of interest.⁴¹

Treatment of GCPM in a mouse model of SNU-16-ffluc cells

Seven days after SNU-16-ffluc cells were implanted into the IP cavity, mice were randomly divided into two treatment groups according to tumor burden average: IP CF33-hNIS-antiPDL1 treatment group (n=8) and IP PBS control group (n=8). Mice in the CF33-hNIS-antiPDL1 treatment group were treated with IP 3×10^5 pfu CF33-hNIS-antiPDL1 in 100 μ L volume on day 7, day 9, and day 11 post tumor cell implantation and were treated for the second time on day 35, day 37, and day 39 with the same amount of virus. Control mice were treated with IP PBS in 100 μ L volume on the same day as the virus-treated group. On day 7 and beyond, tumor burden was verified weekly using bioluminescence imaging for luciferase activity. Mice were observed and evaluated for tumor burden (luciferase imaging of peritoneal tumor and weight of tumor at death), body weight, jaundice, peritoneal ascites, cachexia, and survival. Animals were euthanized if they demonstrated >20% body weight loss, jaundice, peritoneal ascites, cachexia, or inability to groom and eat, as per institutional guidelines.

Statistical analysis

Assay results are expressed as means \pm SEM. Statistical analyses comparing the two groups were performed using paired or unpaired Student's t-test. One-way ANOVA was used for comparison of two groups. All p values were two sided, and p values ≤ 0.05 were deemed significant. Statistical significance for survival studies was performed using Kaplan-Meier survival analysis of the log-rank Mantel-Cox

test. GraphPad Prism V.8 (GraphPad Software, La Jolla, California, USA) was used to calculate statistical values.

RESULTS

CF33-OVs infected and replicated in both intestinal-type and diffuse-type GC cells

First, we determined the infection and replication efficiency of CF33-OVs in both intestinal-type (AGS and MKN-74) and diffuse-type (KATO III, MKN-45, SNU-1, and SNU-16) GC cells by standard plaque assay. We collected cell lysates daily over 3 days from wells infected with either CF33, CF33-GFP, CF33-hNIS- Δ , or CF33-hNIS-antiPDL1 at an MOI of 0.01. Standard viral plaque assays demonstrated that all OVs successfully infected and replicated in the six GC cell lines at an MOI as low as 0.01. The plateau of replication was reached 3 days after infection (figure 1). Comparison of the growth kinetics of CF33 and its derivatives showed that the replacement of two viral genes (*J2R* and *F14.5L*) with two transgenes (hNIS and anti-PD-L1) attenuated growth of this virus compared with the 'wild-type' CF33 or its derivatives with single gene deletions. However, this attenuation in growth seemed to vary in different cell lines. For example, the attenuation was minimal in AGS cells, while it was greatest (about 1 log difference) in MKN-45 cells. Nevertheless, given that the titer of the virus encoding 2 transgenes increased by at least 100-fold within 3 days suggests that the virus retains its oncolytic activity.

CF33 and its derivatives kill GC cells in a dose and time-dependent manner

Next, we compared the cytotoxic ability of these OVs in six human GC cell lines. We infected these cell lines with either CF33, CF33-GFP, CF33-hNIS- Δ , or CF33-hNIS-antiPDL1 at MOIs ranging from 0.01 to 10 over 8 days. CF33-OVs killed GC cells in a dose and time-dependent manner, with greater and faster cell kill at higher MOIs, reaching >90% cell killing within 8 days at MOI 1 and 10 (figure 2). At lower MOIs of 0.01 and 0.1, CF33-hNIS-antiPDL1 demonstrated a lower cytotoxicity curve than unmodified CF33 or single gene inserted CF33-GFP and CF33-hNIS- Δ in accordance with virus replication (figure 1). All CF33-OVs were effective in killing the six GC cell lines (figure 2). Of note, CF33 variants showed lower toxicity against SNU-16 at lower MOIs of 0.01 and 0.1, but there was significant growth inhibition at higher MOIs of 1 and 10 within 8 days. Our results demonstrate that CF33 and its derivatives kill GC cells in a dose and time-dependent manner, and the novel engineered OV, CF33-hNIS-antiPDL1, maintains its oncolytic properties in GC.

GCPM cell lines express CF33-encoded genes after infection

To examine virus-encoded GFP expression, we performed fluorescence imaging of CF33-GFP-infected GC cells, AGS, MKN-74, KATO III, and MKN-45. The time and peak for GFP expression differed in the four cell lines and

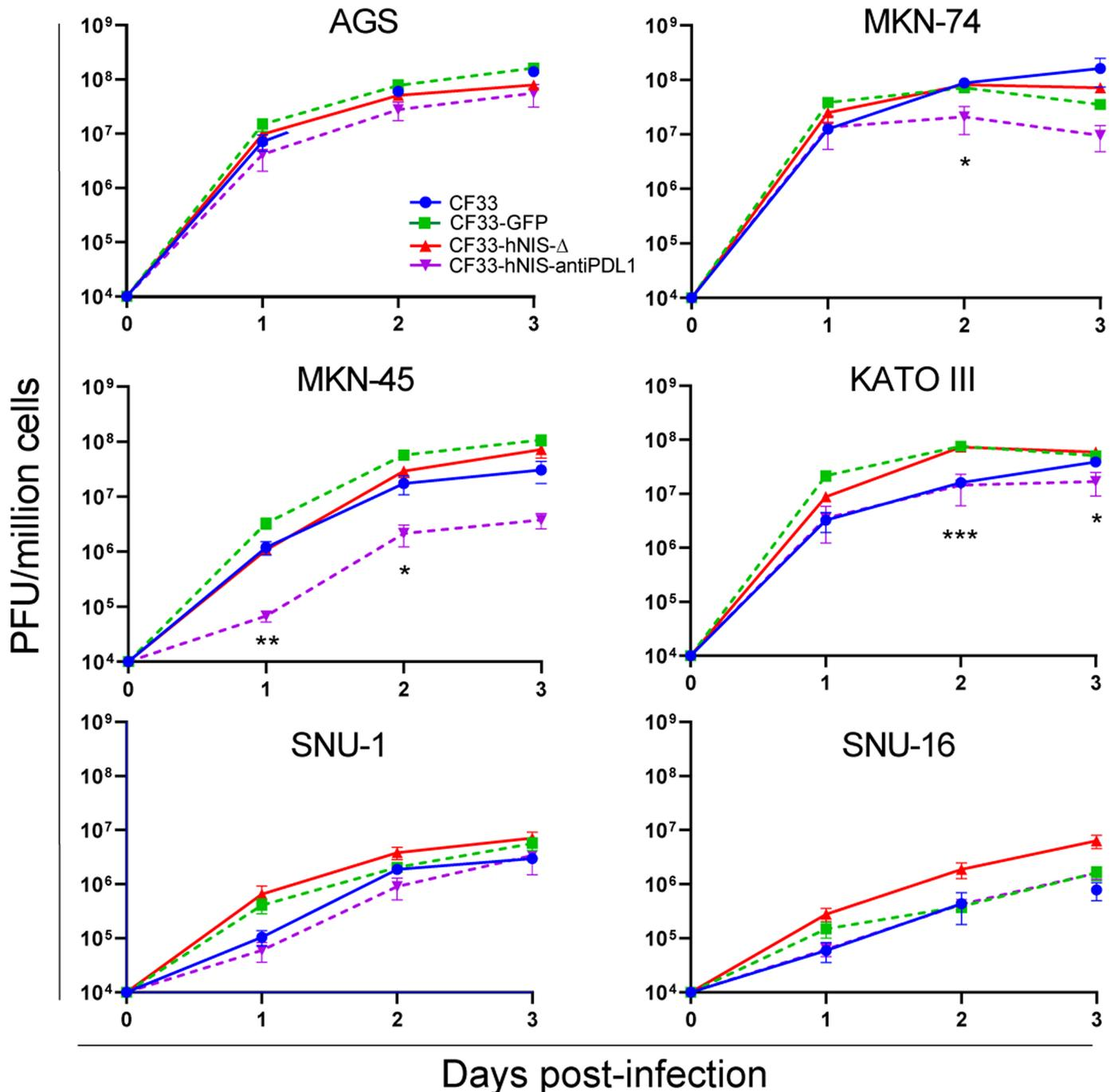


Figure 1 CF33 and its derivatives infect and replicate in human gastric cancer cells. Human intestinal-type (AGS and MKN-74) and diffuse-type (KATO III, SNU-1, SNU-16, and MKN-45) gastric cancer cells infected with either CF33, CF33-GFP, CF33-hNIS- Δ , or CF33-hNIS-antiPDL1 at an MOI of 0.01 were harvested at days 1, 2, and 3 postinfection. Virus titers in the harvested cell lysates were determined using a standard plaque assay. Data are shown as mean \pm SEM. All experiments were performed at least thrice. * p <0.05, ** p <0.01, *** p <0.001, CF33-hNIS-antiPDL1 versus CF33-hNIS- Δ , one-way ANOVA. ANOVA, analysis of variance; MOIs, multiplicities of infection.

for different MOIs tested (figure 3). A slower time to the peak number of infected cancer cells was observed with a lower MOI of 0.01 than a higher MOI of 1 infection.

To test virus-encoded hNIS and anti-PD-L1 scFv expression in GC cells, we treated AGS and MKN-45 cell lines with CF33-hNIS- Δ (MOI=3), CF33-hNIS-antiPDL1 (MOI=3) or PBS control for 18 hours. Fluorescence microscopy showed endogenous NIS expression in some

MKN-45 cells but not in AGS cells (figure 4). Endogenous NIS in stomach cancer cells is not unexpected as NIS is known to exist in the basolateral gastric mucosa in the normal stomach and functions to release I into gastric juices.^{51 52} Variable endogenous expression levels of hNIS in GC and the association between different rates of NIS downregulation with GC prognosis has been reported.⁵² Further, virus-encoded hNIS expression was confirmed

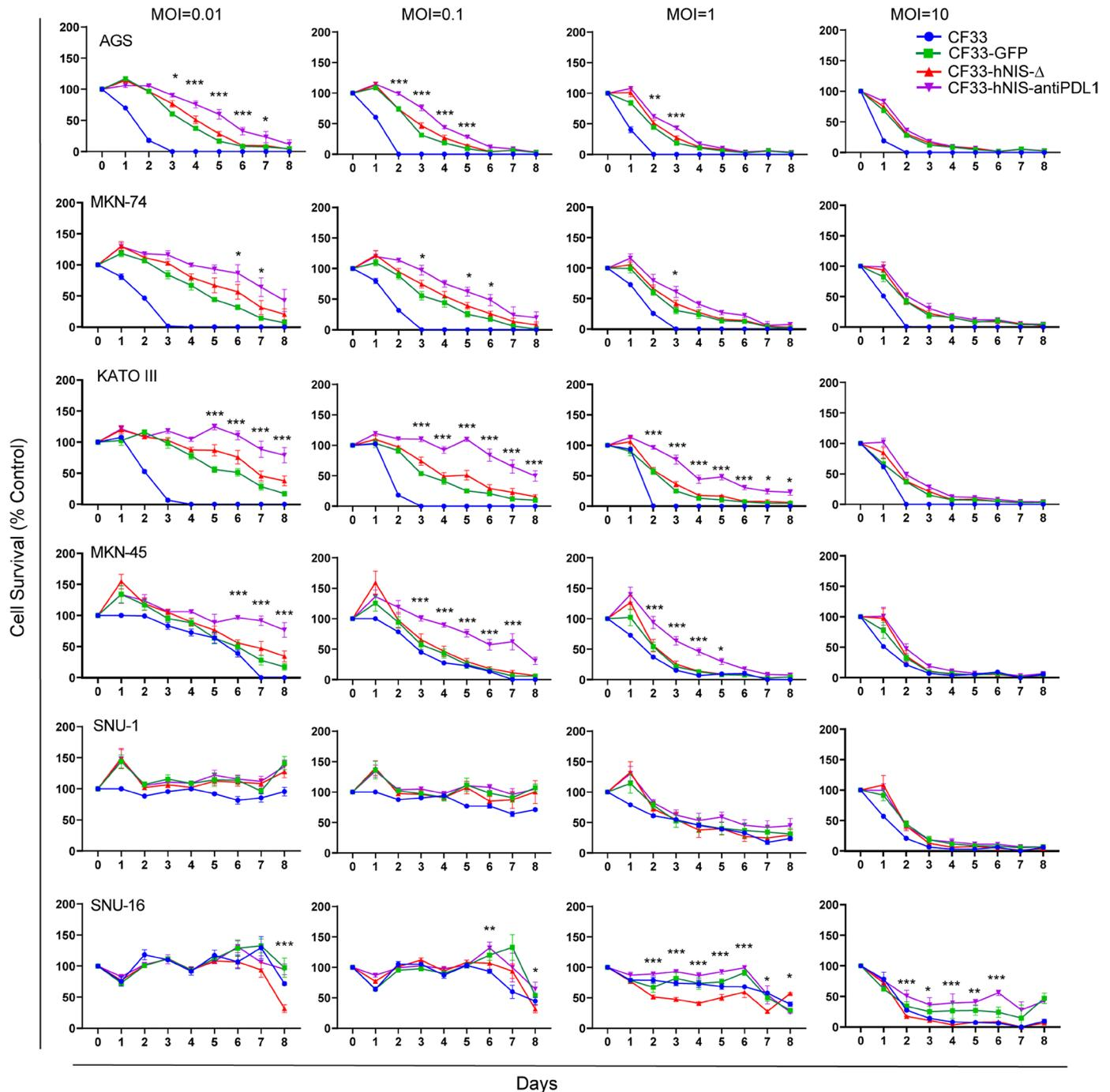


Figure 2 CF33 and its derivatives kill gastric cancer cells. Human intestinal-type (AGS and MKN-74) and diffuse-type (KATO III, SNU-1, SNU-16, and MKN-45) gastric cancer cells were infected with CF33, CF33-GFP, CF33-hNIS- Δ , or CF33-hNIS-antiPDL1 at MOIs 0.01, 0.1, 1, and 10. Cell survival relative to mock-infected cells was calculated daily postinfection for 8 days. Data are shown as mean \pm SEM. All experiments were performed at least thrice. * p <0.05, ** p <0.01, *** p <0.001, CF33-hNIS-antiPDL1 versus CF33-hNIS- Δ , one-way ANOVA. ANOVA, analysis of variance; MOIs, multiplicities of infection.

by immunofluorescence staining following infection with CF33-hNIS- Δ and CF33-hNIS-antiPDL1 but not in the control groups. Anti-PD-L1 scFv with FLAG-tag was observed in the CF33-hNIS-antiPDL1 treated cells but not in the CF33-hNIS- Δ or PBS-treated cells. These results show that CF33-OVs can infect, replicate in, and hijack the genome of the tested GC cell lines and efficiently express virus-encoded GFP, hNIS, and anti-PD-L1 scFv.

GCPM cell lines express cell surface and intracellular CD274/PD-L1

Given that intracellular PD-L1 can be translocated to the cell surface,⁵³ we performed cell surface and intracellular staining of PD-L1 (figure 5). Our analysis showed that five (AGS, KATO III, MKN-74, MKN-45, SNU-1) of the six GC cells had significantly higher expression of CD274 on the cell surface as compared with the isotype controls (p =0.05 or

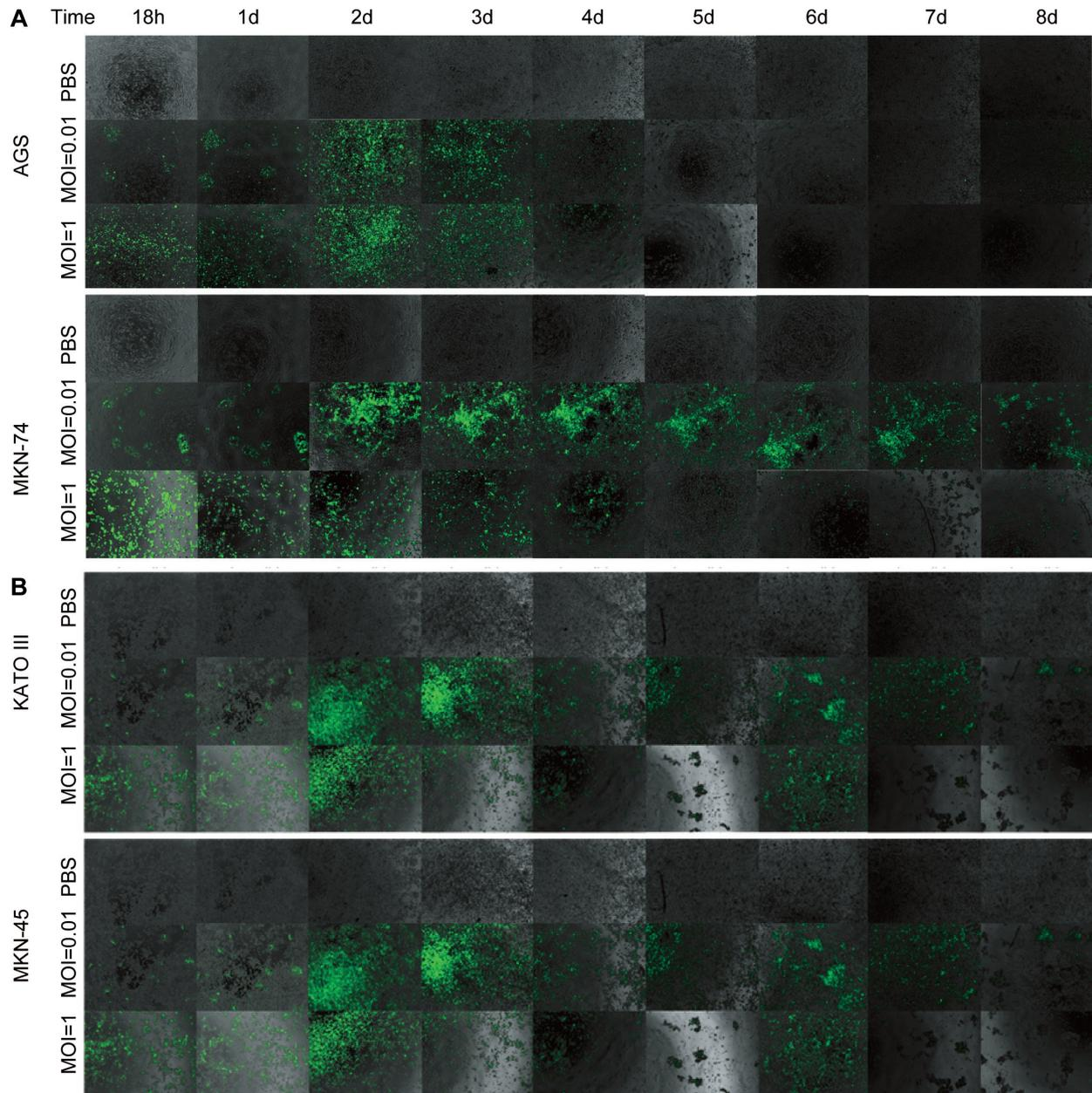


Figure 3 CF33-GFP infection leads to the expression of GFP proteins in gastric cancer cells. Human intestinal-type gastric cancer cells (AGS and MKN-74) (A) and diffuse-type gastric cancer cells (KATO III and MKN-45) (B) were infected with CF33-GFP at MOI=0.01 or MOI=1. Cells were imaged for virus-encoded GFP using a fluorescence microscope at 18 hours and daily postinfection for 8 days. One representative of three independent experiments is shown. MOI, multiplicities of infection; PBS, phosphate buffered saline.

$p < 0.05$) except SNU-16 (figure 5A). As shown in figure 5B, all six GC cell lines showed high intracellular PD-L1 expression compared with intracellular isotype control. These results demonstrate higher baseline intracellular PD-L1 expression than on the cell surface in GCPM cells.

Virus-encoded anti-PD-L1 scFv blocks surface PD-L1/CD274 binding on GC cell lines

Given that abundant intracellular PD-L1 exists in GC cell lines, we analyzed the effect of viral infection on the upregulation of PD-L1 on the cell surface. At 18 hours after CF33-hNIS- Δ (MOI=3) treatment of six GC cell lines, cell surface PD-L1 expression significantly

increased in the AGS and KATO III cell lines, while no change was observed in the MKN-45, MKN-74, SNU-1, and SNU-16 cell lines (figure 6). After treatment of CF33-hNIS-antiPDL1 (MOI=3) for 18 hours, virus-encoded anti-PD-L1 scFv blocked virus-induced PD-L1 upregulation in AGS and KATO III cell lines as well as SNU-16 and MKN-74 cell lines which were not affected by virus treatment. There was no significant difference in blocking of surface PD-L1/CD274 between the control and CF33-hNIS-antiPDL1 groups in MKN-45 and SNU-1 cell lines, likely due to the lower surface expression of PD-L1 in these cells. These results suggest that the anti-PD-L1 scFv

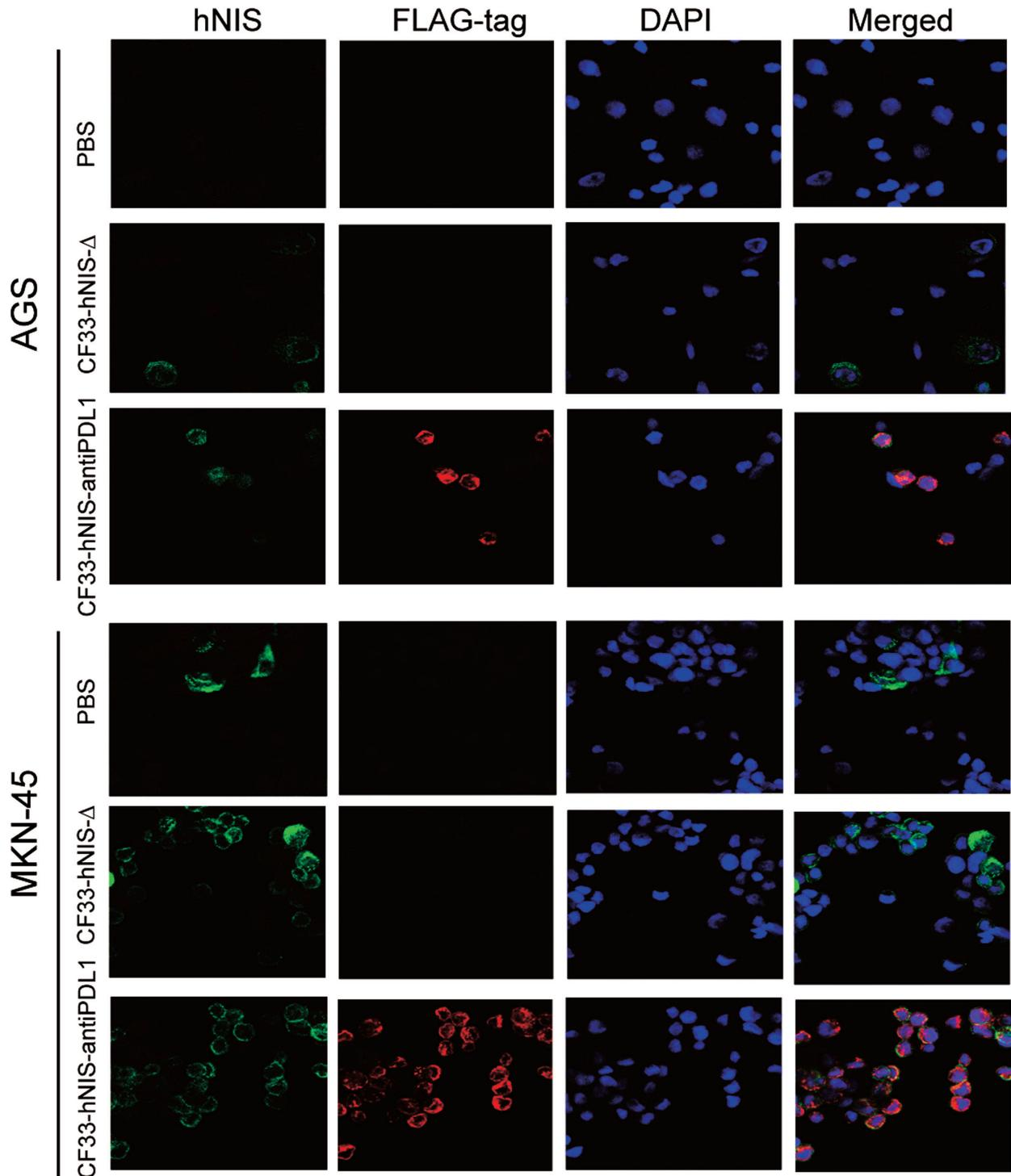


Figure 4 Expression of virus-encoded hNIS and anti-PD-L1 scFv in gastric cancer cells. AGS and MKN-45 cell lines were treated with CF33-hNIS- Δ or CF33-hNIS-antiPDL1 (MOI=3) and evaluated at 18 hours for hNIS and anti-PD-L1 scFv expression by fluorescence microscopy. Virus-encoded hNIS and anti-PD-L1 scFv (FLAG-tag) were observed using Zeiss LSM 880. Note: There is endogenous NIS in the MKN-45 cell line but not in AGS. MOI, multiplicities of infection.

encoded by CF33-hNIS-antiPDL1 is functional and can block cell surface PD-L1 binding in GC cell lines.

CF33-hNIS-antiPDL1 treatment shows antitumor efficacy against a human GCPM xenograft mouse model

Next, we tested the antitumor activity of CF33-hNIS-antiPDL1 in a GCPM xenograft mouse model. We

implanted SNU-16-ffluc cells into the IP cavity of nude mice (figure 7A). After implantation for 7 days, mice were divided into the PBS control group or CF33-hNIS-antiPDL1 treatment group based on the average bioluminescence. Mice were IP treated with either PBS or CF33-hNIS-antiPDL1 on day 7, day 9, and day 11 and

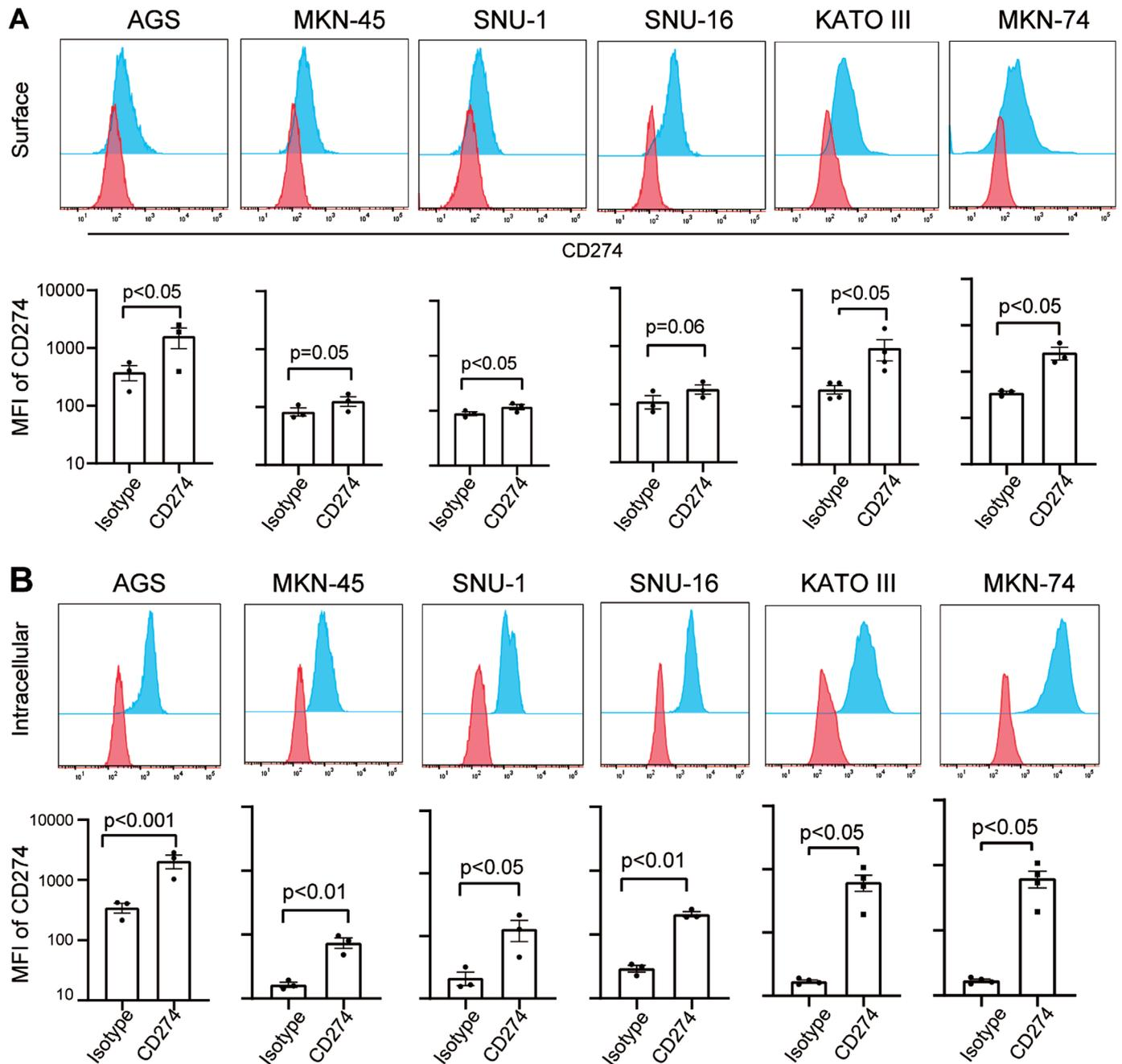


Figure 5 Human gastric cancer cell lines express surface and intracellular CD274/PD-L1. Six gastric cancer cell lines—AGS, MKN-45, SNU-1, SNU-16, KATO III, and MKN-74 were either directly stained (A, surface staining) or fixed/permeabilized, then stained (B, intracellular staining) with PE-anti-PD-L1 antibody or PE-isotype control antibody and analyzed by flow cytometry. (A) The upper row histogram (blue line) shows PD-L1 surface expression levels. The lower row shows MFI (mean fluorescence intensity) of PD-L1 expression compared with isotype control (n=3 or n=4). (B) The upper row histogram (blue line) shows PD-L1 intracellular levels. The lower row shows MFI of PD-L1 expression compared with isotype control (n=3 or n=4). Data are shown as mean±SEM and analyzed using Student's t-test. Surface: surface staining; intracellular: intracellular staining.

also received a second cycle of treatment at the same dosage on day 35, day 37, and day 39 after implantation of SNU-16-fluc. Bioluminescent imaging showed that the CF33-hNIS-antiPD-L1 treated group had the most significant reduction in peritoneal tumor burden at 28 days and 42 days post-treatment compared with the control group (p<0.01 or p<0.0001 IP virus vs control) (figure 7B–D). Mice started to develop symptoms of jaundice and ascites by 55 days post-treatment with PBS.

However, IP CF33-hNIS-antiPD-L1-treated group had a lower number of mice suffering from ascites formation than the control group (CF33-hNIS-antiPD-L1 25.0% vs PBS Control 62.5%). Notably, animals treated with CF33-hNIS-antiPD-L1 demonstrated a lower number of peritoneal tumors, a slower rate of tumor growth, and significantly prolonged survival compared with control animals (p<0.01) (figure 7E). Virus titer analysis (PFU/g organ) for 2 weeks post-treatment did not show the

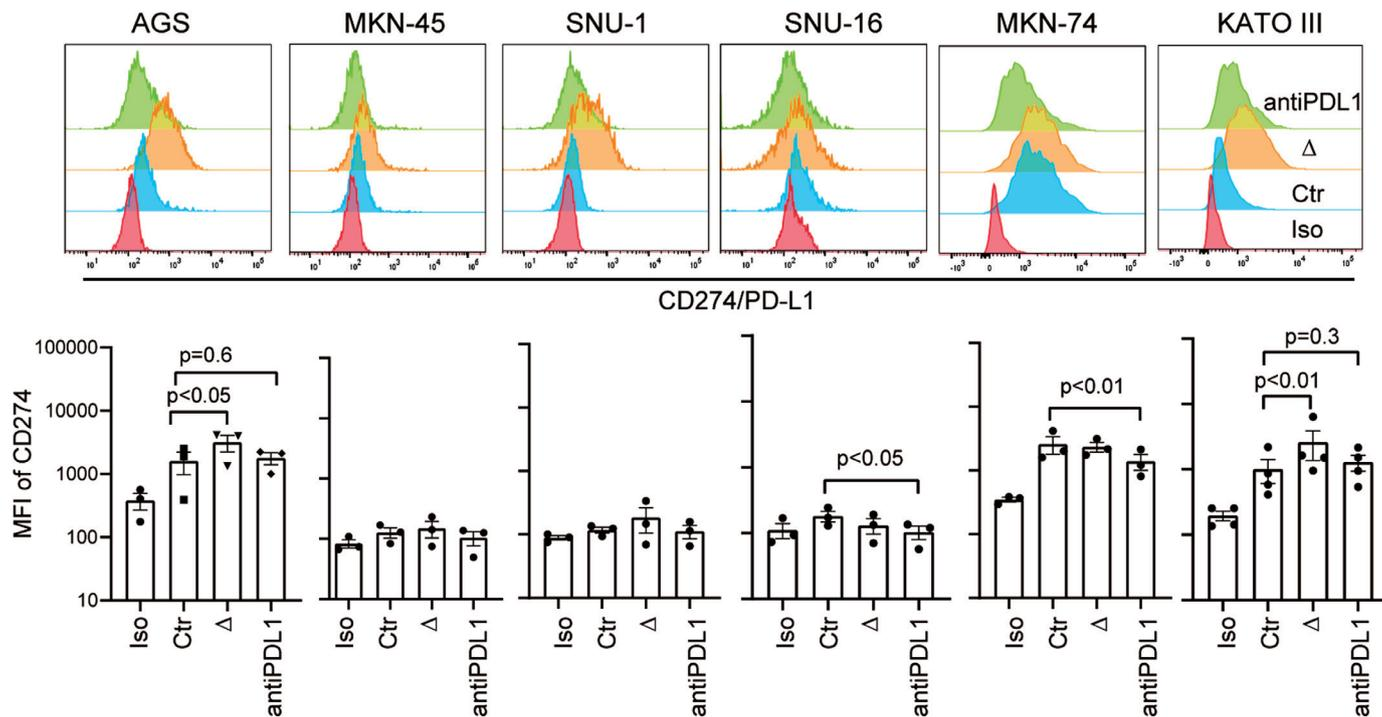


Figure 6 Anti-PD-L1 scFv encoded by the virus blocks CF33-hNIS- Δ -induced surface PD-L1/CD274 binding in gastric cancer cell lines. Six gastric cancer cell lines were treated with CF33-hNIS- Δ or CF33-hNIS-antiPD-L1 (MOI=3) for 15 hours. Exogenous PE-anti-PD-L1 binding to surface PD-L1 was examined using flow cytometric analysis. The upper row shows a representative histogram. The lower row shows MFI (mean fluorescence intensity) of PD-L1 expression compared with the control (n=3 or n=4). Data are shown as mean \pm SEM and analyzed using Student's t-test. Note: Iso=isotype, Ctr=control, Δ =CF33-hNIS- Δ , antiPD-L1=CF33-hNIS-antiPD-L1. MOI, multiplicities of infection.

presence of the virus in the heart, ovary/testis, lung, liver, spleen, kidney, stomach, adrenal gland, intestine, and brain, indicating no off-target toxicity (data not shown). These results demonstrate that IP-delivered CF33-hNIS-antiPD-L1 has significant potential to treat GCPM.

DISCUSSION

In this study, we demonstrate for the first time the exciting therapeutic potential of CF33-OVs against GCPM. CF33-OVs showed robust antitumor activity in both intestinal and diffuse histological types of GC in vitro. Although CF33-hNIS-antiPD-L1 shows a slight decrease in infection, replication, and cytotoxicity, especially with lower MOI, CF33-OVs infected GC cell lines within 3 days and efficiently replicated, increasing the dose of active CF33-OV achieving viral load logs higher than the initial dose. We observed robust and sustained cancer killing of the most sensitive cell line AGS even at the lowest tested MOI of 0.01 with 95% oncolysis within 8 days of treatment. However, the highest tested MOI of 10.0 was required to achieve a similar oncolysis of 97% in the most resistant cell line SNU-16, which was selected for in vivo experiments. We confirmed the expression of functional virus-encoded genes such as GFP, hNIS, and anti-PD-L1 scFv in vitro. Importantly, repeat IP CF33-hNIS-antiPD-L1 was safe and improved survival at doses magnitudes lower than other OVs under investigation. Our preclinical results encourage clinical translation of

CF33-hNIS-antiPD-L1 in the IP treatment of GCPM, which is currently without effective therapies.

Peritoneal metastases (PM) represent an aggressive manifestation of advanced-stage GC, which remains refractory to SOC therapeutic strategies. Peritoneally implanted or unattached tumor cells in the peritoneum associated with or without ascites pose a complex array of therapeutic challenges. The blood-peritoneal barrier and an immunosuppressive TME protect peritoneal tumors and permit immune escape, allowing unchecked peritoneal disease progression. First-line therapy for stage IV GC patients, including those with PM, is systemic chemotherapy with intravenous 5-fluorouracil (5-FU), leucovorin, and oxaliplatin with or without monoclonal antibodies such as trastuzumab (anti-human epidermal growth factor receptor 2), pembrolizumab (anti-programmed cell death 1) and nivolumab (anti-programmed cell death 1). Unfortunately, systemic therapy alone has proven ineffective in GCPM patients failing within the first few treatment cycles. We used the diffuse-type GC, SNU-16, for our in vivo model, which is resistant to 5-FU-based chemotherapeutic regimens. Our data suggest a potential therapeutic role of CF33-hNIS-antiPD-L1 in GCPM patients with chemotherapy-resistant diffuse-type histology.^{54 55} Furthermore, single-agent ICIs, including pembrolizumab and nivolumab, do not provide clinical benefit in GC. However, randomized phase III trials have shown that combination

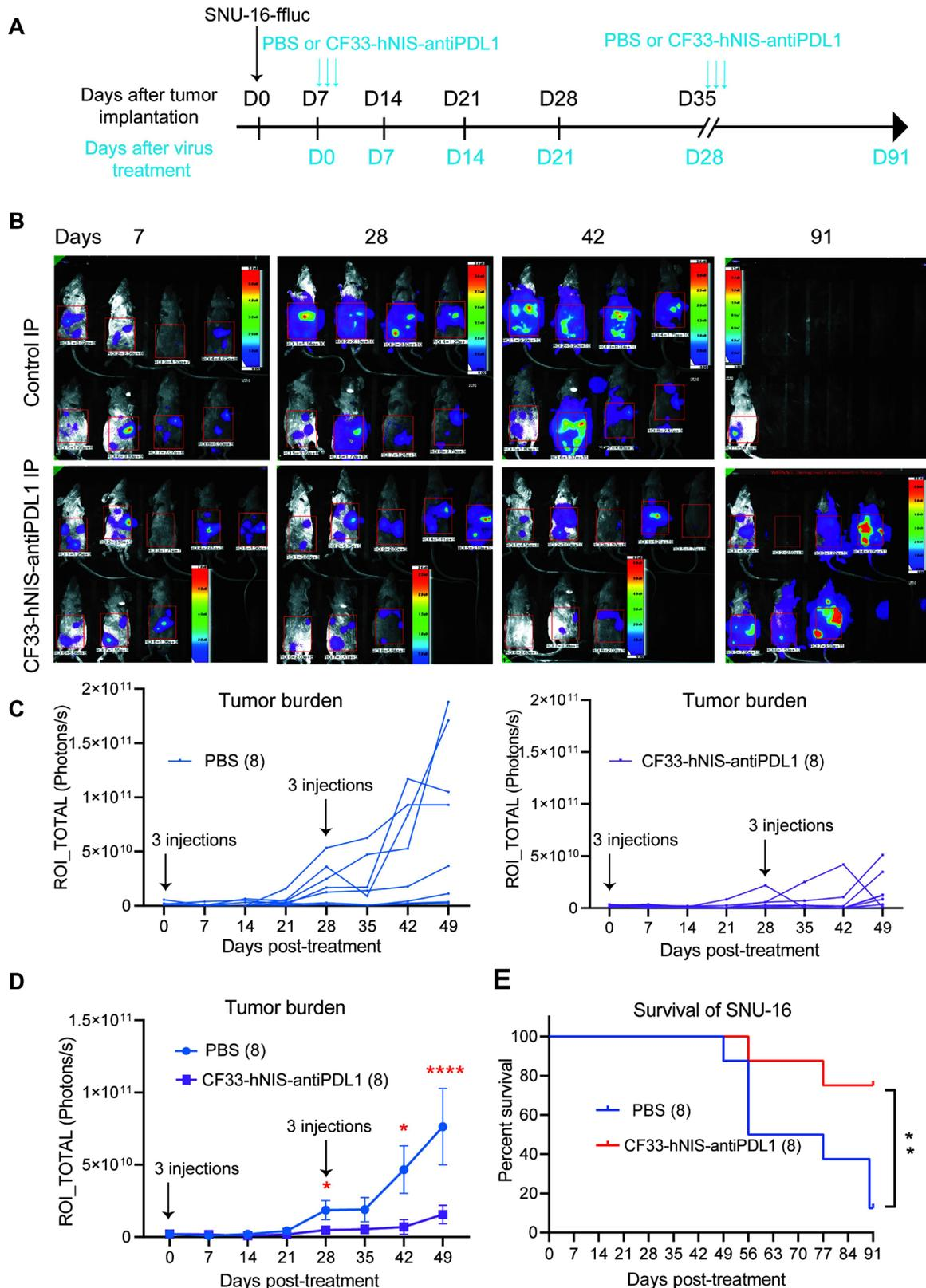


Figure 7 Intraperitoneal CF33-hNIS-antiPDL1 treatment significantly decreases GCPM tumor burden and prolongs survival. (A) The timeline shows intraperitoneal (IP) inoculation of SNU-16-ffluc (10×10^6 cells) in nude mice, IP treatment with CF33-hNIS-antiPDL1 or phosphate buffered saline (PBS), and weekly bioluminescence imaging time points (91 days). Nude mice were IP injected with CF33-hNIS-antiPDL1 or PBS three times (day 7, day 9, and day 11) at a dose of 3×10^5 pfu in 100 μ L PBS post-tumor inoculation and were treated for the second time on day 35, day 37 and day 39 with the same amount of virus. (B) Bioluminescence imaging of the region of interest (ROI) of IP tumor burden. (C) Individual tumor burdens and (D) statistical analysis of tumor burdens (mean \pm SEM, n=8). (E) Kaplan-Meier survival analysis of SNU-16-ffluc peritoneal tumor-bearing mice following treatment with CF33-hNIS-antiPDL1 or PBS control. * $p < 0.05$, ** $p < 0.01$, **** $p < 0.0001$.

therapies that add anti-PD-L1 antibody, pembrolizumab, or nivolumab to SOC chemotherapy enhance antitumor efficacy and improve GC patient survival compared with chemotherapy alone.⁵⁶ While receiving the Food and Drug Administration (FDA) approval as the first line, the significant survival benefit achieved was limited from 1 month to 3.3 months.⁵⁶ Thus, we designed CF33-OVs to deliver anti-PD-L1 to combine the direct oncolytic activity and ICI blockade as a strategy to overcome the distinctly immunosuppressive peritoneal TME and achieve durable responses in patients with intraperitoneally disseminated GC.^{57 58}

Decades of preclinical and early-phase trial results have demonstrated the safety of various OVs, including large DNA viruses such as orthopoxviruses. However, the previous generation of OVs is limited by attenuation of oncolytic activity from genetic modification, high therapeutically effective dosing requirements, and a narrow therapeutic window. To address these limitations, we developed the CF33-OV platform by genetically engineering a chimera of 9 different orthopoxviruses with a preferential tumoricidal activity using high throughput screening against 60 NCI Cancer Cell Panel.^{43 44} CF33-OVs possess a backbone of large DNA genomes. DNA viruses with large genomes are particularly attractive as they can target the cell cycle, harness apoptotic pathways, induce immune responses, and efficiently carry larger human transgenes such as those that encode for hNIS and anti-PD-L1.^{59–61} CF33-OVs can alter the immune TME by activating the host's proinflammatory and immune escape pathways, including affecting PD-L1 expression and function in solid tumors. ICIs, such as anti-PD-1/PD-L1 and anti-CTLA-4, promote antitumor T-cell activation to intervene between immune surveillance and cancer cell proliferation. Combined with OVs, these can outpace the adaptive antiviral immune response and induce a long-lasting antitumor effect, thus boosting efficacy.³⁵ CF33-hNIS-antiPDL1 engineered to express anti-PD-L1 scFv induces immunogenic cell death and carries immune stimulating factors.^{39 40}

Our *in vitro* studies showed that MKN-45, SNU-1, and SNU-16 cells exhibited low cell surface PD-L1 expression levels compared with AGS, KATO-III, and MKN-74. But all cell lines showed high intracellular PD-L1 expression. Cells with low surface expression of PD-L1 will not respond to PD-1/PD-L1 blockade and subsequently not activate cytotoxic T cells. As cell surface upregulation is required to increase PD-L1 targets for anti-PD-L1 antibodies, the low baseline expression levels of PD-L1 in GC may explain why single anti-PD-1/PD-L1 agents, such as pembrolizumab, nivolumab, and avelumab are not superior to chemotherapy in advanced gastric or gastroesophageal junction cancer.⁶² Notably, we demonstrate that virus treatment can upregulate surface PD-L1 expression in AGS and KATO III GC cell lines, consistent with previous reports in breast, colorectal, and pancreatic cancers.^{38 40 63} Moreover, virus-encoded hNIS and anti-PD-L1 scFv with FLAG-tag were verified

by immunofluorescence microscopy, and exogenous PE-conjugated anti-PD-L1 binding to surface PD-L1 was significantly blocked by virus-encoded anti-PD-L1 scFv in AGS, SNU-16, MKN-74, and KATO III cells following CF33-hNIS-antiPDL1 treatment.

The IV, IT, and IP efficacy of CF33-hNIS-antiPDL1 against treatment-resistant tumors was previously demonstrated in pancreatic cancer and TNBC models.^{38 39} While several such OVs, including IP-administered GL-ONC1^{36 59–61} in a phase 1 study of advanced-stage GCPM patients, were well tolerated, their tumor infectivity, viral replication, and tumor lysis were limited. Here, we examined the safety and oncolytic efficacy of CF33-hNIS-antiPDL1 in a xenograft mouse model of GCPM of human SNU-16-*fluc* cells to determine its potential for peritoneal-directed therapy. In our study, the lower doses of CF33-OVs required to achieve GC tumor regression and prolonged animal survival with repeat doses of 3×10^5 pfu demonstrate the safety and potency at lower doses than currently used by other OVs in clinical trials. Moreover, the mice were treated with IP CF33-hNIS-antiPDL1 when tumors were grossly imageable via bioluminescence, reflecting a higher Peritoneal Cancer Index (PCI) score. The virus-treated group had a significantly reduced peritoneal tumor burden, decreased number of mice suffering from ascites formation, and prolonged survival compared with control animals. The dose of the virus used in this study was based on our previous experience with other derivatives of CF33.⁴⁶ We initially planned to administer 3 injections of CF33-hNIS-antiPDL1 at 48 hours intervals (ie, on days 7, 9, and 11 post-tumor implantation). However, by day 35, we saw a clear increase in the BLI (tumor burden) of the virus-treated mice suggesting that the tumor cells could overcome the inhibition posed by the virus after the first round of treatment. Therefore, we decided to administer the virus again on days 35, 37, and 39, based on the T-VEC treatment regimen (the only OV approved in North America), where patients are treated with the second dose 3 weeks after the first injection of the virus.⁶⁴ In patients, OVs are likely to be cleared from the body within a week or 2 after injection, and the antiviral immunity is thought to greatly hinder the efficacy of the subsequent doses, especially for systemically administered OVs. Nevertheless, T-VEC is administered every 2 weeks for up to 6 months. Like T-VEC, which is administered locally (IT), IP injection of CF33-hNIS-antiPDL1 for treating GCPM may be less prone to antibody/complement-mediated neutralization, and multiple rounds of virus injections may be feasible. In the future, we will evaluate multiple rounds of treatments for longer periods in syngeneic models. Taken together, these findings suggest that CF33-hNIS-antiPDL1 has a potential to emerge as a treatment option for GCPM patients with higher peritoneal tumor burden and complications of malignant ascites.

A limitation of our study is that the *in vivo* studies were performed in an immunocompromised human xenograft model of GCPM. While allowing for evaluation of virus safety and efficacy against human GC, it does not

provide information about the additional potential of T cell activation of the anti-PD-L1 scFv expressed by CF33-hNIS-antiPDL1. Moreover, the host immune response to repeat therapy cannot be fully evaluated. Transgenic mouse models are being comprehensively characterized for antitumor and antiviral responses after CF33-OV treatment.

In summary, we show that CF33-OVs can infect, replicate in, express virus-encoded GFP, hNIS and/or anti-PD-L1 scFv, and kill GC cells in vitro. CF33-hNIS-antiPDL1 induces sustained regression of GCPM and prolongs survival following IP delivery in a xenograft mouse model. The promising preclinical antitumor effects of CF33-hNIS-antiPDL1 in GC support peritoneal-directed therapeutic strategies, which are currently lacking in GCPM patients.

Twitter Yuman Fong @SoCalYuman

Acknowledgements Research reported in this publication included work performed in the Analytical Cytometry Core, Light Microscopy Digital Imaging Core, Animal Core facility, and Pathology Core facilities supported by the National Cancer Institute of the National Institutes of Health under grant number P30CA033572. The authors would like to thank Byungwook Kim, Dr. Maria Hahn, Seonah Kang, Austin Santiago and Dr. Colin Cook in our laboratory for technical support and Dr. Supriya Deshpande for assistance with manuscript editing. The authors would also like to thank Dr. Brian Armstrong in Light Microscopy Digital Imaging Core, Lucy Brown in Analytical Cytometry Core, and Drs. Aimin Li and Zhirong Yin in Pathology Core of City of Hope for supporting the work. CF33-hNIS-antiPDL1 (CHEKVAC) and CF33-hNIS (VAXINIA), the CF33-oncolytic viruses discussed in the study have been licensed to Imugene, LTD.

Contributors AY, ZZ, and YW conceived and designed the experiments. AY and ZZ performed the experiments. SC, S-IK, JL, AP, AJ, and SP helped to perform the experiments. AY, ZZ, YF, and YW analyzed and interpreted data. YW and YF secured funding. AY, ZZ, AJ, and YW drafted the manuscript. All authors edited and approved the final manuscript. YW is responsible for the overall content as guarantor, and accepts full responsibility for the finished work and/or the conduct of the study, had access to the data, and controlled the decision to publish.

Funding Department of Defense Idea Award, CA180425 (PI, Yanghee Woo) and Department of Surgery Start-Up Grant City of Hope (PI, Yanghee Woo).

Disclaimer The content is solely the responsibility of the authors and does not necessarily represent the official views of the National Institutes of Health.

Competing interests YW is a member of the scientific advisory board of Imugene LTD; YF owns the patent for CF33-OVs and YF, AP and SP own the patent to CF33-CD19t, both licensed to Imugene LTD. All others have no conflict of interests to declare.

Patient consent for publication Not applicable.

Ethics approval Animal studies were performed under the City of Hope Institutional Animal Care and Use Committee (IACUC)-approved protocol (15003).

Provenance and peer review Not commissioned; externally peer reviewed.

Data availability statement All data relevant to the study are included in the article or uploaded as online supplemental information.

Supplemental material This content has been supplied by the author(s). It has not been vetted by BMJ Publishing Group Limited (BMJ) and may not have been peer-reviewed. Any opinions or recommendations discussed are solely those of the author(s) and are not endorsed by BMJ. BMJ disclaims all liability and responsibility arising from any reliance placed on the content. Where the content includes any translated material, BMJ does not warrant the accuracy and reliability of the translations (including but not limited to local regulations, clinical guidelines, terminology, drug names and drug dosages), and is not responsible for any error and/or omissions arising from translation and adaptation or otherwise.

Open access This is an open access article distributed in accordance with the Creative Commons Attribution Non Commercial (CC BY-NC 4.0) license, which permits others to distribute, remix, adapt, build upon this work non-commercially,

and license their derivative works on different terms, provided the original work is properly cited, appropriate credit is given, any changes made indicated, and the use is non-commercial. See <http://creativecommons.org/licenses/by-nc/4.0/>.

ORCID iDs

Anthony K Park <http://orcid.org/0000-0001-7692-8874>

Saul Priceman <http://orcid.org/0000-0002-8136-2112>

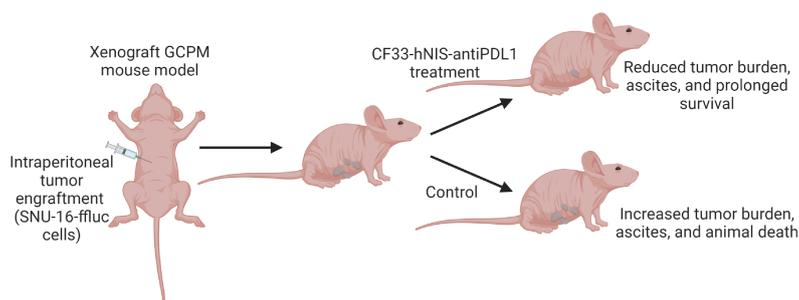
Yanghee Woo <http://orcid.org/0000-0002-6676-0593>

REFERENCES

- Sung H, Ferlay J, Siegel RL, *et al.* Global cancer statistics 2020: GLOBOCAN estimates of incidence and mortality worldwide for 36 cancers in 185 countries. *CA Cancer J Clin* 2021;71:209–49.
- Dicken BJ, Bigam DL, Cass C, *et al.* Gastric adenocarcinoma: review and considerations for future directions. *Ann Surg* 2005;241:27–39.
- Son T, Sun J, Choi S, *et al.* Multi-institutional validation of the 8th AJCC TNM staging system for gastric cancer: analysis of survival data from high-volume eastern centers and the SEER database. *J Surg Oncol* 2019;120:676–84.
- Stewart C, Chao J, Chen Y-J, *et al.* Multimodality management of locally advanced gastric cancer: the timing and extent of surgery. *Transl Gastroenterol Hepatol* 2019;4:42.
- Chuang J, Gong J, Klempner SJ, *et al.* Refining the management of resectable esophagogastric cancer: FLOT4, CRITICS, OE05, MAGIC-B and the promise of molecular classification. *J Gastrointest Oncol* 2018;9:560–72.
- Cheng J, Cai M, Shuai X, *et al.* First-line systemic therapy for advanced gastric cancer: a systematic review and network meta-analysis. *Ther Adv Med Oncol* 2019;11:1758835919877726.
- Desiderio J, Chao J, Melstrom L, *et al.* The 30-year experience—A meta-analysis of randomised and high-quality non-randomised studies of hyperthermic intraperitoneal chemotherapy in the treatment of gastric cancer. *Eur J Cancer* 2017;79:1–14.
- Sirody J, Kaji AH, Hari DM, *et al.* Patterns of gastric cancer metastasis in the united states. *Am J Surg* 2022;224:445–8.
- Green BL, Davis JL. Gastric adenocarcinoma peritoneal carcinomatosis: a narrative review. *Dig Med Res* 2022;5:37.
- Rijken A, Lurvink RJ, Luyer MDP, *et al.* The burden of peritoneal metastases from gastric cancer: A systematic review on the incidence, risk factors and survival. *J Clin Med* 2021;10:4882.
- Nadler A, McCart JA, Govindarajan A. Peritoneal carcinomatosis from colon cancer: a systematic review of the data for cytoreduction and intraperitoneal chemotherapy. *Clin Colon Rectal Surg* 2015;28:234–46.
- Cancer Genome Atlas Research Network. Comprehensive molecular characterization of gastric adenocarcinoma. *Nature* 2014;513:202–9.
- Cristescu R, Lee J, Nebozhyn M, *et al.* Molecular analysis of gastric cancer identifies subtypes associated with distinct clinical outcomes. *Nat Med* 2015;21:449–56.
- Kim ST, Sa JK, Oh SY, *et al.* Comprehensive molecular characterization of gastric cancer patients from phase II second-line ramucicromab plus paclitaxel therapy trial. *Genome Med* 2021;13:11.
- Ichikawa H, Nagahashi M, Shimada Y, *et al.* Actionable gene-based classification toward precision medicine in gastric cancer. *Genome Med* 2017;9:93.
- Shen W, Wang G, Cooper GR, *et al.* The epithelial and stromal immune microenvironment in gastric cancer: A comprehensive analysis reveals prognostic factors with digital cytometry. *Cancers (Basel)* 2021;13:5382.
- Lin Y, Huang K, Cai Z, *et al.* A novel exosome-relevant molecular classification uncovers distinct immune escape mechanisms and genomic alterations in gastric cancer. *Front Pharmacol* 2022;13:884090.
- Kus T, Kose F, Aktas G, *et al.* Prediction of peritoneal recurrence in patients with gastric cancer: a multicenter study. *J Gastrointest Cancer* 2021;52:634–42.
- Ji L, Selleck MJ, Morgan JW, *et al.* Gastric cancer peritoneal carcinomatosis risk score. *Ann Surg Oncol* 2020;27:240–7.
- Koemans WJ, Lurvink RJ, Grootsholten C, *et al.* Synchronous peritoneal metastases of gastric cancer origin: incidence, treatment and survival of a nationwide dutch cohort. *Gastric Cancer* 2021;24:800–9.
- Rau B, Brandl A, Piso P, *et al.* Peritoneal metastasis in gastric cancer: results from the German database. *Gastric Cancer* 2020;23:11–22.
- Bang Y-J, Van Cutsem E, Feyereislova A, *et al.* Trastuzumab in combination with chemotherapy versus chemotherapy alone for treatment of HER2-positive advanced gastric or gastro-oesophageal

- junction cancer (ToGA): a phase 3, open-label, randomised controlled trial. *Lancet* 2010;376:687–97.
- 23 Wilke H, Muro K, Van Cutsem E, *et al.* Ramucirumab plus paclitaxel versus placebo plus paclitaxel in patients with previously treated advanced gastric or gastro-oesophageal junction adenocarcinoma (rainbow): a double-blind, randomised phase 3 trial. *Lancet Oncol* 2014;15:1224–35.
- 24 Xu R-H, Zhang Y, Pan H, *et al.* Efficacy and safety of weekly paclitaxel with or without ramucirumab as second-line therapy for the treatment of advanced gastric or gastroesophageal junction adenocarcinoma (RAINBOW-asia): a randomised, multicentre, double-blind, phase 3 trial. *Lancet Gastroenterol Hepatol* 2021;6:1015–24.
- 25 Fuchs CS, Tomasek J, Yong CJ, *et al.* Ramucirumab monotherapy for previously treated advanced gastric or gastro-oesophageal junction adenocarcinoma (regard): an international, randomised, multicentre, placebo-controlled, phase 3 trial. *Lancet* 2014;383:31–9.
- 26 Shitara K, Van Cutsem E, Bang Y-J, *et al.* Efficacy and safety of pembrolizumab or pembrolizumab plus chemotherapy vs chemotherapy alone for patients with first-line, advanced gastric cancer: the KEYNOTE-062 phase 3 randomized clinical trial. *JAMA Oncol* 2020;6:1571–80.
- 27 Fuchs CS, Doi T, Jang RW, *et al.* Safety and efficacy of pembrolizumab monotherapy in patients with previously treated advanced gastric and gastroesophageal junction cancer: phase 2 clinical KEYNOTE-059 trial. *JAMA Oncol* 2018;4:e180013.
- 28 Janjigian YY, Kawazoe A, Yañez P, *et al.* The KEYNOTE-811 trial of dual PD-1 and HER2 blockade in HER2-positive gastric cancer. *Nature* 2021;600:727–30.
- 29 Wang R, Song S, Harada K, *et al.* Multiplex profiling of peritoneal metastases from gastric adenocarcinoma identified novel targets and molecular subtypes that predict treatment response. *Gut* 2020;69:18–31.
- 30 Ruiz Hispán E, Pedregal M, Cristobal I, *et al.* Immunotherapy for peritoneal metastases from gastric cancer: rationale, current practice and ongoing trials. *J Clin Med* 2021;10:4649.
- 31 Muro K, Chung HC, Shankaran V, *et al.* Pembrolizumab for patients with PD-L1-positive advanced gastric cancer (KEYNOTE-012): a multicentre, open-label, phase 1b trial. *Lancet Oncol* 2016;17:717–26.
- 32 Kang Y-K, Boku N, Satoh T, *et al.* Nivolumab in patients with advanced gastric or gastro-oesophageal junction cancer refractory to, or intolerant of, at least two previous chemotherapy regimens (ONO-4538-12, ATTRACTION-2): a randomised, double-blind, placebo-controlled, phase 3 trial. *Lancet* 2017;390:2461–71.
- 33 Bang Y-J, Cho JY, Kim YH, *et al.* Efficacy of sequential ipilimumab monotherapy versus best supportive care for unresectable locally advanced/metastatic gastric or gastroesophageal junction cancer. *Clin Cancer Res* 2017;23:5671–8.
- 34 Rogers JE, Xiao L, Trail A, *et al.* Nivolumab in combination with irinotecan and 5-fluorouracil (FOLFIRI) for refractory advanced gastroesophageal cancer. *Oncology* 2020;98:289–94.
- 35 Lichty BD, Breitbach CJ, Stojdl DF, *et al.* Going viral with cancer immunotherapy. *Nat Rev Cancer* 2014;14:559–67.
- 36 Mell LK, Brumund KT, Daniels GA, *et al.* Phase I trial of intravenous oncolytic vaccinia virus (GL-ONC1) with cisplatin and radiotherapy in patients with locoregionally advanced head and neck carcinoma. *Clin Cancer Res* 2017;23:5696–702.
- 37 Park SH, Breitbach CJ, Lee J, *et al.* Phase 1B trial of biweekly intravenous pexa-vec (JX-594), an oncolytic and immunotherapeutic vaccinia virus in colorectal cancer. *Mol Ther* 2015;23:1532–40.
- 38 Chaurasiya S, Yang A, Zhang Z, *et al.* A comprehensive preclinical study supporting clinical trial of oncolytic chimeric poxvirus CF33-hnis-anti-PD-L1 to treat breast cancer. *Mol Ther Methods Clin Dev* 2022;24:102–16.
- 39 Woo Y, Zhang Z, Yang A, *et al.* Novel chimeric immuno-oncolytic virus CF33-hnis-antipdl1 for the treatment of pancreatic cancer. *J Am Coll Surg* 2020;230:709–17.
- 40 Zhang Z, Yang A, Chaurasiya S, *et al.* CF33-hnis-antipdl1 virus primes pancreatic ductal adenocarcinoma for enhanced anti-PD-L1 therapy. *Cancer Gene Ther* 2022;29:722–33.
- 41 Zhang Z, Yang A, Chaurasiya S, *et al.* PET imaging and treatment of pancreatic cancer peritoneal carcinomatosis after subcutaneous intratumoral administration of a novel oncolytic virus, CF33-hnis-antipdl1. *Mol Ther Oncolytics* 2022;24:331–9.
- 42 Warner SG, Kim S-I, Chaurasiya S, *et al.* A novel chimeric poxvirus encoding hnis is tumor-tropic, imageable, and synergistic with radioiodine to sustain colon cancer regression. *Mol Ther Oncolytics* 2019;13:82–92.
- 43 O’Leary MP, Choi AH, Kim S-I, *et al.* Novel oncolytic chimeric orthopoxvirus causes regression of pancreatic cancer xenografts and exhibits abscopal effect at a single low dose. *J Transl Med* 2018;16:110.
- 44 O’Leary MP, Warner SG, Kim S-I, *et al.* A novel oncolytic chimeric orthopoxvirus encoding luciferase enables real-time view of colorectal cancer cell infection. *Mol Ther Oncolytics* 2018;9:13–21.
- 45 Chaurasiya S, Chen NG, Lu J, *et al.* A chimeric poxvirus with J2R (thymidine kinase) deletion shows safety and anti-tumor activity in lung cancer models. *Cancer Gene Ther* 2020;27:125–35.
- 46 Chaurasiya S, Yang A, Kang S, *et al.* Oncolytic poxvirus CF33-hnis- δ 14.5 favorably modulates tumor immune microenvironment and works synergistically with anti-PD-L1 antibody in a triple-negative breast cancer model. *Oncotarget* 2020;9:1729300.
- 47 Zhang Z, Shively JE. Generation of novel bone forming cells (monoosteophils) from the cathelicidin-derived peptide LL-37 treated monocytes. *PLoS One* 2010;5:e13985.
- 48 Priceman SJ, Gerdtts EA, Tilakawardane D, *et al.* Co-stimulatory signaling determines tumor antigen sensitivity and persistence of CAR T cells targeting PSCA+ metastatic prostate cancer. *Oncotarget* 2018;7:e1380764.
- 49 Contero A, Richer E, Gondim A, *et al.* High-throughput quantitative bioluminescence imaging for assessing tumor burden. *Methods Mol Biol* 2009;574:37–45.
- 50 Klerk CPW, Overmeer RM, Niers TMH, *et al.* Validity of bioluminescence measurements for noninvasive in vivo imaging of tumor load in small animals. *Biotechniques* 2007;43:7–13.
- 51 Ravera S, Reyna-Neyra A, Ferrandino G, *et al.* The sodium/iodide symporter (NIS): molecular physiology and preclinical and clinical applications. *Annu Rev Physiol* 2017;79:261–89.
- 52 Altorjay Áron, Dohán O, Szilágyi A, *et al.* Expression of the Na⁺/I⁻ symporter (NIS) is markedly decreased or absent in gastric cancer and intestinal metaplastic mucosa of Barrett esophagus. *BMC Cancer* 2007;7:5.
- 53 Xiong W, Gao Y, Wei W, *et al.* Extracellular and nuclear PD-L1 in modulating cancer immunotherapy. *Trends Cancer* 2021;7:837–46.
- 54 Pádua D, Barros R, Amaral AL, *et al.* A Sox2 reporter system identifies gastric cancer stem-like cells sensitive to monensin. *Cancers* 2020;12:495.
- 55 Ku JL, Park JG. Biology of SNU cell lines. *Cancer Res Treat* 2005;37:1–19.
- 56 Janjigian YY, Shitara K, Moehler M, *et al.* First-line nivolumab plus chemotherapy versus chemotherapy alone for advanced gastric, gastro-oesophageal junction, and oesophageal adenocarcinoma (CheckMate 649): a randomised, open-label, phase 3 trial. *Lancet* 2021;398:27–40.
- 57 Thomassen I, van Gestel YR, van Ramshorst B, *et al.* Peritoneal carcinomatosis of gastric origin: a population-based study on incidence, survival and risk factors. *Int J Cancer* 2014;134:622–8.
- 58 Glimelius B, Ekström K, Hoffman K, *et al.* Randomized comparison between chemotherapy plus best supportive care with best supportive care in advanced gastric cancer. *Ann Oncol* 1997;8:163–8.
- 59 Thorne SH. Immunotherapeutic potential of oncolytic vaccinia virus. *Front Oncol* 2014;4:155.
- 60 Jun K-H, Gholami S, Song T-J, *et al.* A novel oncolytic viral therapy and imaging technique for gastric cancer using a genetically engineered vaccinia virus carrying the human sodium iodide symporter. *J Exp Clin Cancer Res* 2014;33:2.
- 61 Lauer UM, Schell M, Beil J, *et al.* Phase I study of oncolytic vaccinia virus GL-ONC1 in patients with peritoneal carcinomatosis. *Clin Cancer Res* 2018;24:4388–98.
- 62 Wang B-C, Zhang Z-J, Fu C, *et al.* Efficacy and safety of anti-PD-1/PD-L1 agents vs chemotherapy in patients with gastric or gastroesophageal junction cancer: a systematic review and meta-analysis. *Medicine (Baltimore)* 2019;98:e18054.
- 63 Kim S-I, Park AK, Chaurasiya S, *et al.* Recombinant orthopoxvirus primes colon cancer for checkpoint inhibitor and cross-prime T cells for antitumor and antiviral immunity. *Mol Cancer Ther* 2021;20:173–82.
- 64 Rehman H, Silk AW, Kane MP, *et al.* Into the clinic: talimogene laherparepvec (T-VEC), a first-in-class intratumoral oncolytic viral therapy. *J Immunother Cancer* 2016;4:53.

Development of the Oncolytic Virus, CF33 and its Derivatives for Peritoneal-Directed Treatment of Gastric Cancer Peritoneal Metastases



Authors

Annie Yang, Zhifang Zhang, Shyambabu Chaurasiya, Anthony K. Park, Audrey Jung, Jianming Lu, Sang-In Kim, Saul Priceman, Yuman Fong, Yanghee Woo

Correspondence

yhwoo@coh.org, zh Zhang@coh.org

In Brief

CF33-OVs demonstrate robust in vitro and in vivo antitumor effects in GCPM models. Intraperitoneal delivery of CF33-hNIS-antiPDL1 leads to tumor regression and prolonged animal survival in a xenograft GCPM mouse model.